Radon Transform Orientation Estimation for Rotation Invariant Texture Analysis

Kourosh Jafari-Khouzani, [1,2]
Hamid Soltanian-Zadeh, [1,3] *Senior Member, IEEE*

Technical Report TR-0105
Jan. 12, 2005

Kourosh Jafari-Khouzani
Radiology Image Analysis Lab.
Henry Ford Health System
One Ford Place, 2F (Box 82)
Detroit, MI 48202

Phone Number: (313) 874-4378
Fax Number: (313) 874-4494
E-mail: kjafari@rad.hfh.edu

Hamid Soltanian-Zadeh
Radiology Image Analysis Lab.
Henry Ford Health System
One Ford Place, 2F (Box 82)
Detroit, MI 48202

Phone Number: (313) 874-4482
Fax Number: (313) 874-4494
E-mail: hamids@rad.hfh.edu

[1] Radiology Image Analysis Lab, One Ford Place, 2F, Henry Ford Health System, Detroit, MI 48202, USA.
[2] Department of Computer Science, 431 State Hall, Wayne State University, Detroit, MI 48202, USA.
[3] Dept. of Electrical and Computer Eng., University of Tehran, Tehran, 14395-515, Iran

Radon Transform Orientation Estimation for Rotation Invariant Texture Analysis

Kourosh Jafari-Khouzani and Hamid Soltanian-Zadeh, *Senior Member, IEEE*

Abstract--**This paper presents a new approach to rotation invariant texture classification. The proposed approach benefits from the fact that most of the texture patterns either have directionality (anisotropic textures) or are not with a specific direction (isotropic textures). The wavelet energy features of the directional textures change significantly when the image is rotated. However, for the isotropic images, the wavelet features are not sensitive to rotation. Therefore, for the directional textures it is essential to calculate the wavelet features along a specific direction. In the proposed approach, the Radon transform is first employed to detect the principal direction of the texture. Then, the texture is rotated to place its principal direction at 0°. A wavelet transform is applied to the rotated image to extract texture features. This approach provides a features space with small intra-class variability and therefore good separation between different classes. The performance of the method is evaluated using three texture sets. Experimental results show the superiority of the proposed approach compared with some existing methods.**

Index Terms--**Texture classification, Radon transform, wavelet transform, rotation invariance**.

I. INTRODUCTION

Texture analysis plays an important role in computer vision and image processing. The applications include medical imaging, remote sensing, content-based image retrieval, and document segmentation. Translation, rotation, and scale invariant texture analysis methods have been of particular interest [1]. In this paper, we are concerned with the rotation invariant texture classification problem.

So far, many attempts have been directed towards rotation invariant texture analysis [1], including polarogram [2], circular symmetric autoregressive random field (CSAR) model [3], and rotation invariant SAR model [4]. Pietikainen, et al. [5] present a set of features to describe the texture, most of which locally invariant to rotation. Ojala, et al. [6] employ binary patterns defined on circularly symmetric neighborhood sets. In all of these methods, a neighborhood is utilized, which only captures the local intensity variations of the texture and overlooks the global information.

Circular-Mellin features [7] are created by decomposing the image into a combination of harmonic components in its polar form and are shown to be rotation and scale invariant. Zernike moments [8] are used to create rotation, scale and illumination invariant color texture characterization. Greenspan, et al. [9] use the steerable pyramid model to get rotation invariance. Cohen, et al. [10] model texture as Gaussian Markov random field and use the maximum likelihood technique to estimate the coefficients and rotation angles. Chen and Kundu [11] use multichannel subband decomposition and a hidden Markov model to solve the problem.

Multiresolution approaches such as Gabor filters, wavelet transforms, and wavelet frames have been widely studied and used for texture characterization. Wavelets provide spatial/frequency information of textures, which are useful for classification and segmentation. However, wavelet

transform is not translation and rotation invariant. Several attempts have been made towards using the wavelet transform for rotation invariant texture analysis. Some of the proposed methods use a preprocessing step to make the analysis invariant to rotation or use rotated wavelets and exploit the steerability to calculate the wavelet transform for different orientations to achieve invariant features. Pun and Lee [12] apply log-polar transform and then use an invariant wavelet transform to create rotation and scale invariant features. Manthalkar, et al. [13] combine LH and HL channels of the wavelet decomposition to get rotation invariant features. Charalampidis and Kasparis [14] use wavelet-based roughness features and steerability to get rotation invariance.

Haley and Manjunath [15] employ a complete space-frequency model using Gabor wavelets to achieve a rotation-invariant texture classification. Wu and Wei [16] create 1-D signals by sampling the images along a spiral path and use a quadrature mirror filter bank to decompose the signals into subbands and calculate several features for each subband. Do and Vetterli [17] use a steerable wavelet-domain hidden Markov model and a maximum likelihood estimator to find the model parameters. Campisi, et al. [18] model the texture as the output of a linear system driven by a binary image. The features extracted from the autocorrelation function of the binary image are used for classification of the texture. In a previous paper [19] we apply translation invariant wavelet transform on Radon transform of the image to create rotation invariant features.

In this paper, the wavelet features are calculated along an estimated orientation. This is similar to manual texture analysis when we rotate the unknown texture to match one of the known textures. There are techniques in the literature to estimate the orientation of the image including methods based on image gradients [20], angular distribution of signal power in the Fourier domain [21],[22] and signal autocorrelation structure [20]. Due to the inherent properties of the Radon transform, it is a useful tool to capture the directional information of the images. Radon transform has been widely used in image analysis. Magli, et al. [23] use Radon transform and 1-D continuous wavelet transform to detect linear patterns in the aerial images. Warrick and Delaney [24] use a localized Radon transform with a wavelet filter to accentuate the linear and chirp-like features in SAR images. Leavers [25] uses the Radon transform to generate a taxonomy of shape for the characterization of abrasive powder particles. Do and Vetterli [26] use ridgelet transform, which is a combination of finite Radon transform and 1-D discrete wavelet transform, to approximate and denoise the images with straight edges. Ridgelet transform is also used to implement curvelet decomposition, which is used for image denoising [27].

The proposed technique employs the Radon transform to capture the directional information and adjust the orientation of the texture for feature extraction. Analyzing textures along their principal directions allows creation of features with smaller intra-class variability, thus allowing higher separability. The outline of the paper is as follows: In Section II, we briefly review the Radon transform and its properties in finding the direction of the texture. In Section III, we present our rotation invariant texture classification approach. Experimental results are presented in Section IV and conclusions are given in Section V.

II. RADON TRANSFORM ORIENTATION ESTIMATION

Radon transform is the fundamental tool used in the proposed approach. In this section, we briefly review this transform and its application in estimating texture direction.

A. Radon Transform

The Radon transform of a 2-D function $f(x, y)$ is defined as:

$$R(r,q)[f(x,y)] = \int_{-\infty}^{\infty}\int_{-\infty}^{\infty} f(x,y)\,d(r - x\cos q - y\sin q)\,dxdy \tag{1}$$

where r is the perpendicular distance of a line from the origin and q is the angle between the line and the y-axis (see Fig. 1). According to the Fourier slice theorem, this transformation is invertible and the 1-D Fourier transforms of the Radon transform along r are the 1-D radial samples of the 2-D Fourier transform of $f(x, y)$ at the corresponding angles [28] (see Fig. 1).

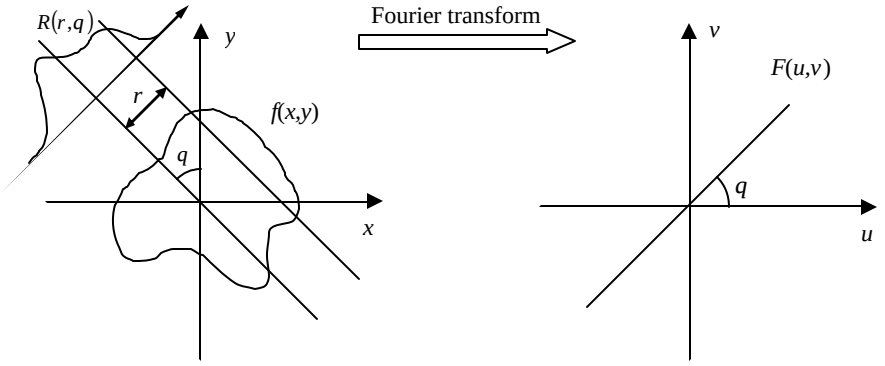

(a) (b)

Fig. 1. (a) Radon transform of the image. (b) 1-D Fourier transforms of the projections construct the 2-D Fourier transform of the image.

B. Texture Orientation

Wavelet transform has been widely used for texture classification in the literature. However, it is not rotation invariant. The reason being is that textures have different frequency components along different orientations. Ordinary wavelet transform captures the variations along specific directions (namely horizontal, vertical, and diagonal), due to the separability of the wavelet basis functions. Fig. 2 shows a directional (anisotropic) texture sample from Brodatz album (D53) in two different orientations and their Fourier transforms. The Fourier transform rotates as the image rotates. As shown, the Fourier transform changes significantly when the image is rotated. However, some textures have no specific direction (isotropic textures). This means the frequency components of the texture do not change significantly at different orientations. In other words, its Fourier transform is almost circularly symmetric. Therefore, the wavelet features are approximately invariant to rotation.

Fig. 3 shows an isotropic texture sample from Brodatz album (D66) in two different orientations and their Fourier transforms. As shown, the Fourier transform does not significantly change when the image is rotated. Fig. 4 shows the wavelet energy features (mean square of wavelet coefficients in each subband) for textures D53 and D66 at orientations 0° to 160° with 20° increments. The energy features are calculated from the wavelet coefficients produced by four levels of ordinary wavelet decomposition (therfore creating 13 subbands) using Daubechies wavelet of length 2 (db_2). The features are numbered from 1 to 13 with smaller numbers

corresponding to lower frequency subbands. Feature 1 is divided by 10 in order to be shown with the other features in the figure. Comparing Figs. 4(a) and 4(b) we observe that the wavelet features of the anisotropic texture (D53 in Fig. 4(a)) have larger variations compared with the isotropic texture (D66 in Fig. 4(b)) when the orientation of the texture changes.

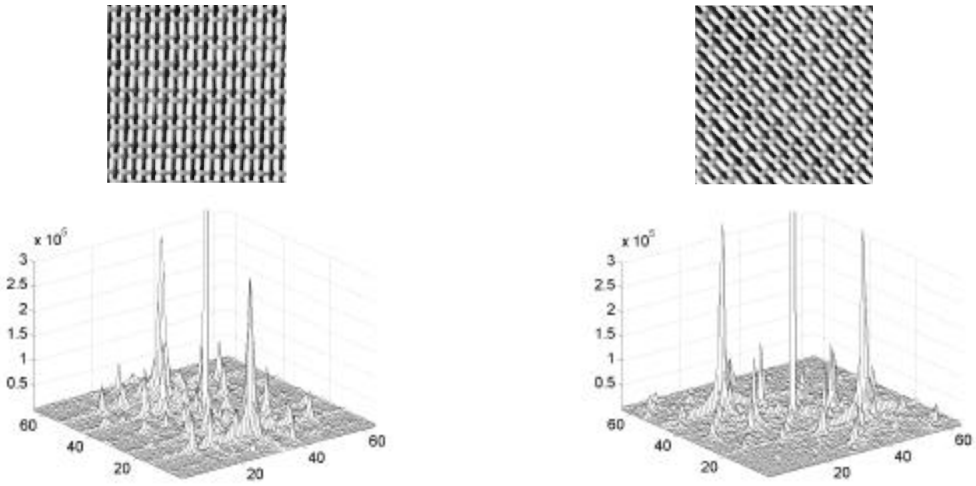

Fig. 2. A directional texture (D53) in two different orientations and their Fourier transforms. Note that Fourier transform changes significantly when the image is rotated.

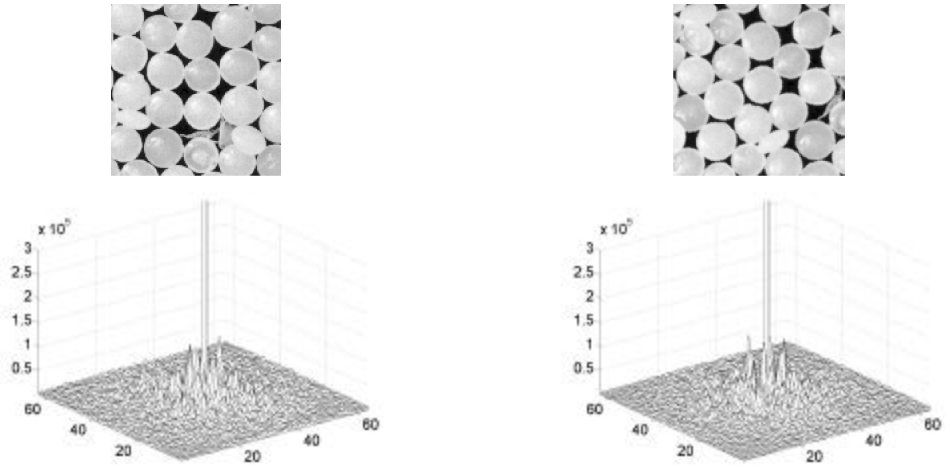

Fig. 3. An isotropic texture (D66) in two different orientations and their Fourier transforms. Note that the frequency components of the texture are not significantly different at different orientations. In other words, its Fourier transform is almost circularly symmetric.

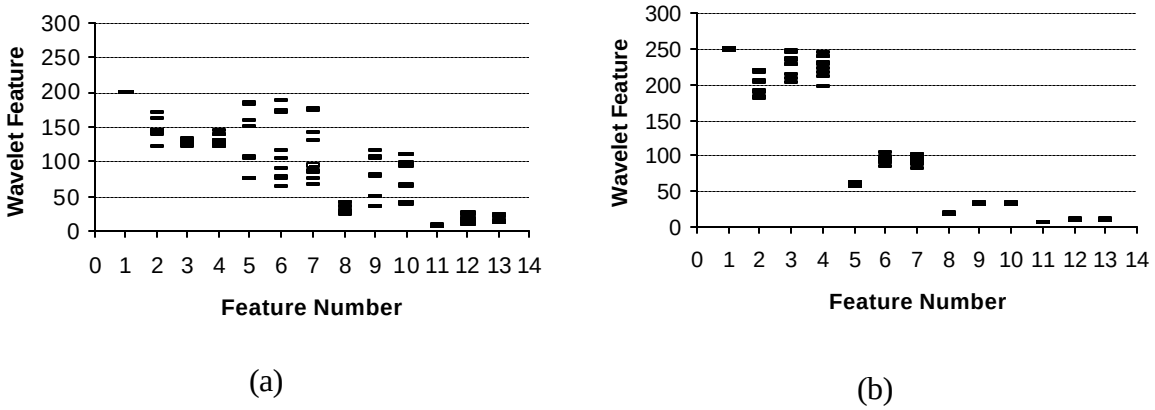

Fig. 4. Wavelet energy features for two different textures at orientations from 0° to 160° with 20° increments. (a) D53 which is a directional texture, and (b) D66 which is an isotropic texture. Note that, the wavelet features of the directional texture has larger variations compared with the isotropic texture.

This motivates us to find a principal direction for each texture and calculate the wavelet features along this direction to achieve rotation invariance. The basic tool we propose is the Radon transform. The Radon transform can be used to detect linear trends in images. Texture principal direction can be roughly defined as the direction along which there are more straight lines. The Radon transform along this direction usually has larger variations. Therefore, the variance of the projection at this direction is locally maximum.

Fig. 5 (a) and (b) show an anisotropic (directional) texture and the variance of the projections along different orientations. A disk shape area from the middle of the image has been selected before calculating the Radon transform to make the method isotropic. As shown, the variance of the projections has two local maxima at 45° and 135° (with vertical direction at 0°). The local maximum at 45° is narrower compared with the local maximum at 135°, because there are more straight lines along 45°. Thus, the derivative[1] of the variance changes more rapidly at 45° (see Fig. 5(c)). To distinguish between these two local maxima, we may calculate the second derivative of the variance, which has its minimum at 45°. This is depicted in Fig. 5(d).

This technique may accurately find the texture direction for structural textures like the one shown in Fig. 5. Furthermore, since taking the derivative removes the low frequency components of the variance, this method is robust to illumination changes across the image. This method has an advantage over techniques that use the contributions of all frequencies in the Fourier domain [21],[22]. In practice, the angular energy distribution may change significantly in a texture. Therefore, it is not always reliable to find the dominant orientation using the contributions of all frequencies. Fig. 6 shows this using two samples of texture D105 from Bordatz album at different orientations (20° and 60°) along with the variances of projections and their second derivatives. As shown, although the angular energy distributions are different, the estimations based on the second derivative are accurate.

[1] In this paper, the derivative of a signal sequence is estimated by the difference of successive values.

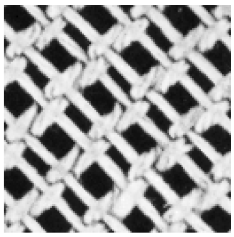

(a)

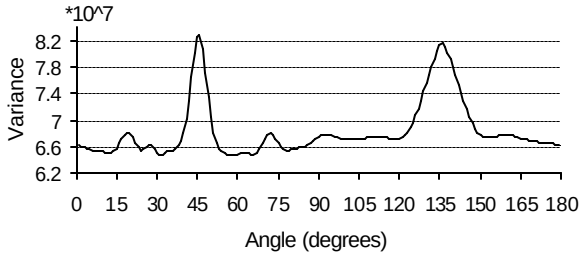

(b)

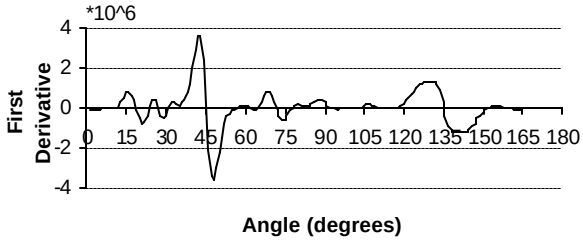

(c)

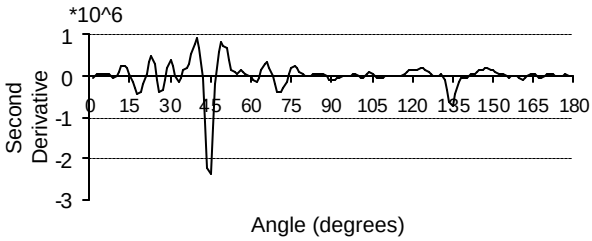

(d)

Fig. 5. (a) A directional texture rotated at 45°, (b) the variance of projections at different angles, (c) first derivative of (b), (d) second derivative of (b). Note that the variance of the projections has two local maxima at 45° and 135° (with vertical direction at 0°). The local maximum at 45° is narrower compared with the local maximum at 135°, because there are more straight lines along 45°.

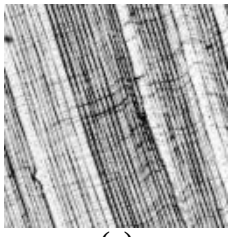

(a)

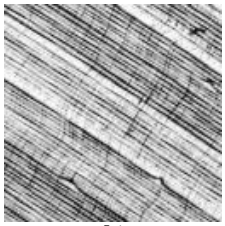

(b)

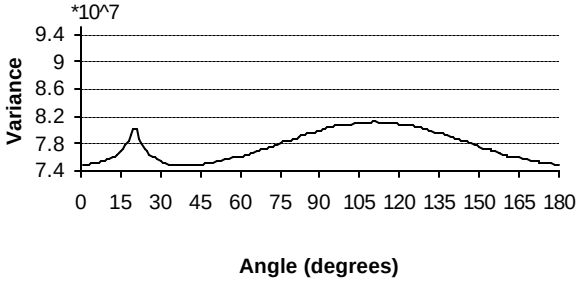

(c)

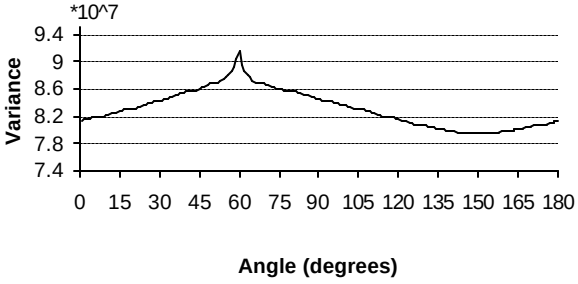

(d)

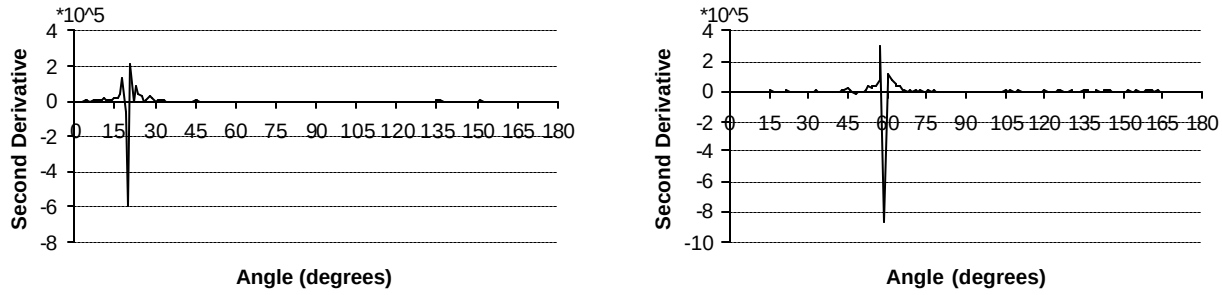

(e) (f)

Fig. 6. A directional texture with principal directions of (a) 20° and (b) 60°. (c), (d) the variances of the projections. (e), (f) the second derivatives of the variances. As shown, although the angular energy distributions are different, the estimations based on the second derivative are accurate.

III. PROPOSED METHOD

Fig. 7 shows a block diagram of the proposed method. As shown, the principal direction of the image is first estimated from the Radon transform of a disk shape area of the image. The image is then rotated to move the principal direction to 0°. A wavelet transform is employed to extract texture features. The image is finally classified using a k-NN classifier. In the following, these steps are explained.

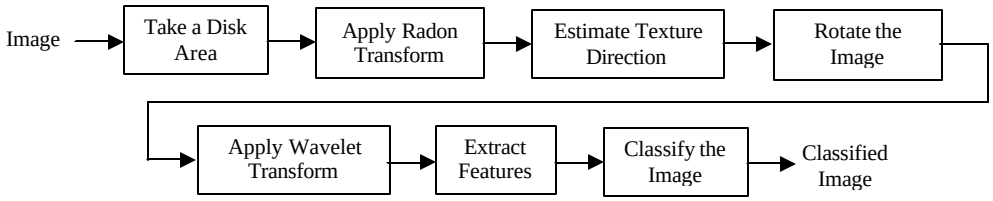

Fig. 7. Block diagram of the proposed rotation invariant texture classification technique.

A. Orientation Adjustment

To estimate the orientation of the texture, a disk shape area is selected in the center of the image. The Radon transform is calculated for angles between 0° and 180°. Based on the theory presented in Section II, the orientation of the texture is estimated as follows.

$$\alpha = \arg\left(\min_{q} \frac{d^2 s_q^2}{dq^2} \right) \tag{2}$$

where $s_q^2 = 1/N \sum_r \left(R(r,q) - m_q\right)^2$ is the variance of the projection at q, $m_q = 1/N \sum_r R(r,q)$, and N is the number of samples in each projection. Then we rotate the image by $-\alpha$ to adjust the orientation of the texture.

B. Wavelet Feature Extraction

By applying the wavelet transform to the rotated image, a number of subbands are produced. For each subband I^s, we calculate the following features:

$$e_1 = \frac{1}{M \times N} \sum_{i=1}^{M} \sum_{j=1}^{N} \left| I_{i,j}^{s} \right| \tag{3}$$

$$e_2 = \frac{-1}{\log(M \times N)} \sum_{i=1}^{M} \sum_{j=1}^{N} \frac{\left| I_{i,j}^{s} \right|}{\text{anorm}} \log\left(\frac{\left| I_{i,j}^{s} \right|}{\text{anorm}} \right) \tag{4}$$

where $\text{anorm} = \sum_{i,j} \left| I_{i,j}^{s} \right|$, M and N are the dimensions of each subband, and s represents the subband number. The features e_1 and e_2 are similar to the energy and entropy features with the difference of using absolute values instead of squared values. The energy and entropy features have been shown to be useful for texture analysis [11],[12].

Note that the wavelet transform is calculated for a disk shape area of the image. The sharp edges of its circular boundary affect the wavelet features. But since this is the case for all the images, it has equal effect for all the texture features in each class. Therefore, it does not have significant impact on the classification.

C. Classification

We use the k-nearest neighbors (k-NN) classifier with Euclidean distance to classify each image into an appropriate class. Since different features have different ranges of possible values, the classification may be based primarily on the features with wider ranges of values. For this reason, before classification, we normalize each feature using the following formula:

$$\hat{f}_{i,j} = \frac{f_{i,j} - m_j}{s_j} \tag{5}$$

where $f_{i,j}$ is the jth feature of the ith image, and m_j and s_j are the mean and variance of the feature j in the training set.

On the other hand, the features may not have the same level of significance for classification. Therefore, we apply a feature selection technique to choose the best combination of features and improve the classification. In this paper, we apply weights to the normalized features. The weight for each feature is calculated as the correct classification rate in the training set (a number between 0 and 1) using only that feature and the leaving-one-out technique [29]. This is based on the sense that the features with higher discrimination power deserve higher weights, which is similar to matched filtering. Although this method may not provide an optimal weight vector but is sensible and straightforward to implement.

D. Robustness to Additive Noise

The proposed method to estimate the principal direction is robust to additive noise. It has been shown that signal to noise ratio increases after applying the Radon transform [19]. Suppose the image is denoted by $\hat{f}(x,y) = f(x,y) + h(x,y)$ where $h(x,y)$ is white noise with zero mean and

variance s_n^2. Let $\hat{p}_r = R(r,q)\left[\hat{f}(x,y)\right]$, then $\hat{p}_r = \hat{p}_{r,s} + \hat{p}_{r,n}$ where $\hat{p}_{r,s}$ and $\hat{p}_{r,n}$ are respectively the Radon transforms of the signal and noise at orientation q. Thus:

$$\mathrm{var}(\hat{p}_r) = \mathrm{var}(p_{r,s}) + \mathrm{var}(p_{r,n}) + 2\,\mathrm{cov}(p_{r,s}, p_{r,n}) \tag{6}$$

$$E[\mathrm{var}(\hat{p}_r)] = E[\mathrm{var}(p_{r,s})] + E[\mathrm{var}(p_{r,n})] + 2E[\mathrm{cov}(p_{r,s}, p_{r,n})] \tag{7}$$

According to the formulas derived in [19]:

$$E[\mathrm{var}(p_{r,s})] = \frac{pN_R}{2}s^2 + \frac{8}{3}m^2N_R^2 - \left(\frac{pN_R}{2}m\right)^2 \tag{8}$$

$$E[\mathrm{var}(p_{r,n})] \approx \frac{pN_R}{2}s_n^2 \tag{9}$$

where m and s^2 are mean and variance of signal $f(x,y)$ and N_R is the radius of the image disk area in terms of pixels.

Usually $\frac{8}{3}m^2N_R^2 >> pN_R s_n^2/2$ and if we assume the additive white noise and image are uncorrelated, the term $2E[\mathrm{cov}(p_{r,s}, p_{r,n})]$ is negligible compared with $E[\mathrm{var}(p_{r,s})]$. Therefore, the difference of $E[\mathrm{var}(\hat{p}_r)] - E[\mathrm{var}(p_{r,s})]$ is small compared with $E[\mathrm{var}(p_{r,s})]$. This shows that the additive white noise has a small effect on the variance of projection and therefore the estimation of the principal texture direction, i.e., the estimation is robust to additive white noise. Fig. 8 shows the variances of the projections of a sample texture (D06) before and after adding zero mean white Gaussian noise with the signal to noise ratio (SNR) of 0db. As shown, noise has little effect on the variances (changes the variances on the order of 1% while preserving the overall shape of the signal).

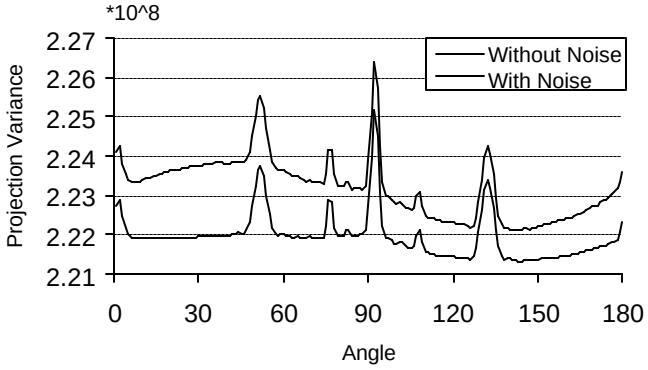

Fig. 8. The variances of the projections before and after white Gaussian noise addition with SNR=0db. As shown, noise has little effect on the variances (changes the variances on the order of 1% while preserving the overall shape of the signal).

E. Fast Technique for Orientation Estimation

Using the Fourier slice theorem, there is an alternative method to determine the texture principal direction. According to this theorem, the 1-D Fourier transform of the projection of $f(x, y)$ at q is equal to the 1-D radial samples of the 2-D Fourier transform of $f(x, y)$ at the corresponding angle. On the other hand, the signal energy is the same in the time and frequency domains according to the Parseval's theorem:

$$\int_{-\infty}^{\infty} R^2(r,q)dr = \int_{-\infty}^{\infty} F_q^2(s)ds \tag{10}$$

where $F_q(s)$ is the 1-D radial sample of the Fourier transform of $f(x, y)$. Thus,

$$s_q^2 = \int_{-\infty}^{\infty} (R(r,q) - m_q)^2 dr = \int_{-\infty}^{\infty} R^2(r,q)dr - m_q^2 = \int_{-\infty}^{\infty} F_q^2(s)ds + c \tag{11}$$

where c is independent of q because m_q is independent of q. Therefore,

$$a = \arg\left(\min_q \frac{d^2 s_q^2}{dq^2} \right) = \arg\left(\min_q \frac{d^2}{dq^2} \int_{-\infty}^{\infty} F_q^2(s)ds \right) \tag{12}$$

Hence, we may calculate the Fourier transform of the image and use its 1-D radial samples to calculate s_q^2. However, since in practice we have discrete Fourier transform and most of the energy is located around the origin in the frequency domain, more samples are needed around the origin to have accurate calculations. Zero padding may be used to generate more samples of the Fourier transform. In addition, fast algorithms that calculate the polar Fourier transform of an image of size $N \times N$ in $O(N^2 \log N)$ [30] can be used.

IV. EXPERIMENTAL RESULTS

We demonstrate the efficiency of the proposed approach using three data sets. Data set 1 consists of 25 texture images of size 512×512 from Brodatz album [31] used in [12]. We divided each texture image into four 256×256 nonoverlapping regions. Then, we extracted one 128×128 subimage from the middle of each region to create a training set of 100 (25×4) images. To create the test set, each 256×256 region was rotated at angles 10º to 160º with 10º increments and from each rotated image one 128×128 subimage was selected (the subimages were selected off center to make minimum overlap for different angles). With this approach, we created a total number of 1600 (25×4×16) for the testing set (approximately 6% for training and 94% for testing).

In the experiments, to estimate the principal direction we calculate the Radon transform for angles 0° to 180° with 0.5° increments. Fig. 9 shows the error mean and square root of mean square (SRMS) error of the direction estimation for each texture in the testing set. The error is defined as the difference between the estimated orientations of each two successive rotated textures (which is supposed to be 10°) minus 10. The estimated errors are corrected based on the fact that few textures like D21 have two symmetric principal directions with 90° difference (either of them is correct). The SRMS error of directional and isotropic textures are displayed as solid and dashed bars, respectively. The mean values of the errors are shown by dotted bars. As

shown, the error power is large for the isotropic textures. However, this error does not affect the classification rate, since as mentioned earlier, the extracted wavelet features do not change significantly when an isotropic texture is rotated. On the other hand, the errors for the directional textures are significantly smaller than those for the isotropic textures. In this figure, the mean and standard deviation of the SRMS of errors for the directional textures are 1.15 and 3.49 degrees, respectively. Moreover, note that the estimated error is higher than the real error because sometimes the texture direction changes within the texture pattern (e.g. D22, D103, and D105). Except for D22 and D102, the error is very low (less than 1°) for directional textures. The reason D22 has high error is that it has three symmetric principal directions (see Fig. 10 (a)). Similarly, D102 has two non-symmetric principal directions (see Fig. 10 (b)). We can also observe that the error mean is small for most of the textures, which means the estimation method is unbiased for most of the textures.

Using the proposed method, we calculated the wavelet features for the training and testing images. For data set 1, we used four levels of ordinary wavelet decomposition with different wavelet bases. The three most high-resolution subbands were ignored as they were dominated by noise. Thus, the features were calculated from 10 submatrices. A k-NN classifier was employed to classify each texture based on the extracted features. The classification results are presented in Table 1. The results are reported for different k values in the k-NN classifier before and after applying the weights to the features. As shown, applying the weights has generated higher improvement on e_2 compared with e_1. The best classification rate is 98.8% using 20 features after applying the weights, compared with the maximum of 93.8% in [12] using 64 features. Nevertheless, a direct comparison between the results of our proposed method and the method presented in [12] is not possible due to the difference between the classifiers. A Mahalanobis classifier is used in [12], with all the images at different orientations for both training and testing, while we used the images at 0º for training (6%) and all the other orientations for testing (94%). Using db_6 wavelet, we even get 98.6% using only 10 features. Table 2 shows the confusion map when we have the maximum of 98.8% classification rate in Table 1. In this table, only the textures with non-zero error are shown.

In Table 3, we have also presented the classification rates using two alternative methods: (1) local binary patterns ($LBP^{riu2}_{P,R}$ features) [6] and k-NN classifier, and (2) the proposed method in [19] using db_2 wavelet. As shown, the maximum classification rates for these methods are 88.9% and 92.1% compared with the maximum of 98.8% with the proposed method.

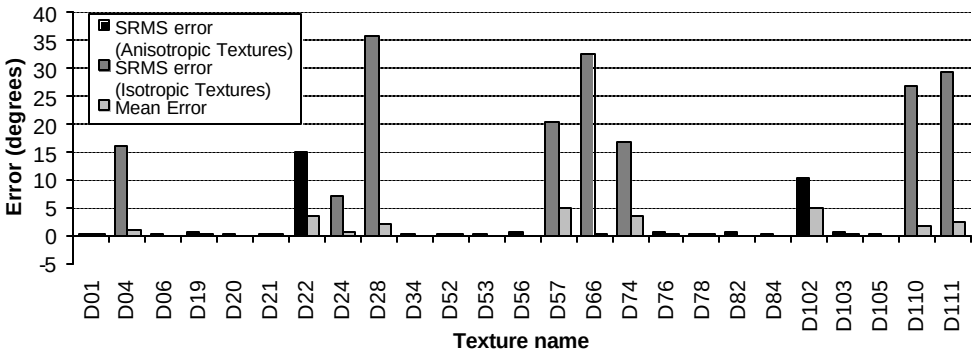

Fig. 9. The SRMS and means of estimation errors. The values for the directional textures are shown by solid bars, for the isotropic textures are shown by dashed bars and the error

means are shown by dotted bars. Note that except for D22 and D102, the errors are very small (less than 1°) for the directional textures.

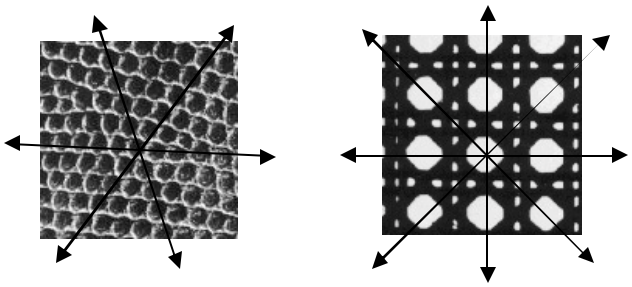

(a) (b)

Fig. 10. The textures (a) D22 and (b) D102 which have multiple principal directions.

Table 1. The correct classification percentages for data set 1 using the proposed method with different wavelet bases, feature sets, and k values for k-NN classifier.

Wavelet Bases	Features	k					
		1	3	5	1	3	5
		Before Weight			After Weight		
db_2	e_1	97.8	95.9	88.9	96.8	95.9	87.8
	e_2	75.9	68.1	64.8	80.3	75.1	70.8
	e_1 & e_2	96.8	96.3	91.5	97.9	98.0	91.2
db_4	e_1	96.4	96.8	90.8	96.1	97.1	88.6
	e_2	76.3	69.3	68.0	79.7	75.1	70.3
	e_1 & e_2	97.5	97.3	92.9	97.8	98.2	92.4
db_6	e_1	98.2	95.8	89.1	98.6	97.5	88.8
	e_2	66.2	57.1	57.4	69.9	64.6	62.5
	e_1 & e_2	96.7	94.3	89.3	**98.8**	98.1	92.1
db_8	e_1	96.1	94.4	89.6	97.1	95.8	88.6
	e_2	58.1	48.5	50.4	62.3	53.9	51.3
	e_1 & e_2	93.4	92.1	87.2	97.9	96.9	92.5
db_{12}	e_1	95.8	94.3	87.6	98.2	97.3	86.6
	e_2	52.6	41.8	44.1	55.4	50.5	51.9
	e_1 & e_2	89.4	84.3	80.8	98.2	98.3	90.8

Table 2. The confusion map for the maximum classification rate of 98.8% in Table 1. To minimize the table size, textures classified 100% correctly are not listed.

	D04	D20	D24	D52	D76	D111
D04	63		1			
D20		63			1	
D24	14		50			
D52				61		3

Table 3. The correct classification percentages for data set 1 using local binary patterns and the method proposed in [19] with different k values in the k-NN classifier.

Feature	P,R	k					
		1	3	5	1	3	5
		Before Weight			After Weight		
$LBP^{riu2}_{P,R}$	8,1	40.8	38.9	36.0	44.9	43.7	41.8
	16,2	81.6	80.3	72.6	83.0	82.4	75.9
	24,3	88.6	86.9	83.1	**88.9**	87.9	83.9
	8,1+16,2	76.4	72.8	65.3	82.4	77.9	71.2
	8,1+24,3	87.3	86.7	82.1	88.1	88.3	83.6
	16,2+24,3	87.3	87.3	81.8	87.8	87.9	83.1
	8,1+16,2+24,3	86.5	85.8	81.2	88.0	88.6	82.6
Proposed method in [19] with db_2 wavelet	e_1	90.4	86.3	81.6	90.1	86.3	79.0
	e_2	56.9	55.7	56.5	68.2	68.1	68.0
	e_1 & e_2	81.6	79.6	77.1	**92.1**	88.1	84.3

To evaluate the robustness of the direction estimation method to additive white noise, we compared the estimated directions before and after adding white Gaussian noise with SNR=0db. Defining the error as the difference between these two estimations, the means and SRMS of errors are displayed in Fig. 11. As shown, noise does not have significant effect on the orientation estimation of directional textures. In this figure, the mean and standard deviation of the SRMS of errors for the directinal textures are 1.75° and 3.44°, respectively. The textures D19, D22, D56, D76 and D102 have larger errors, due to either multiple principal directions or weak staight lines that are significantly affected by the additive noise.

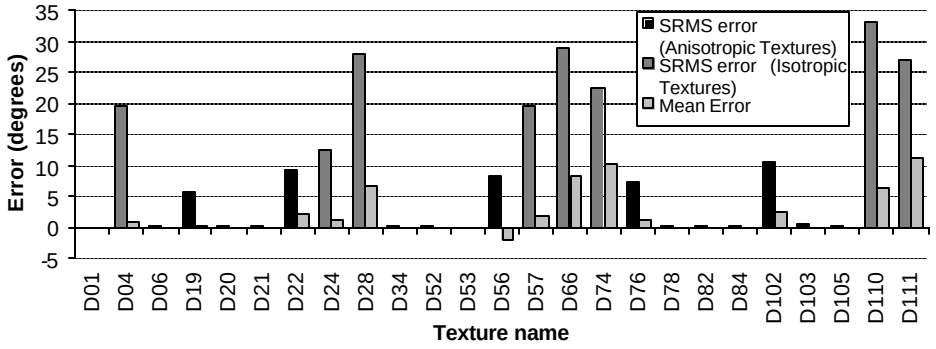

Fig. 11. The SRMS and means of differences between the estimated orientations before and after adding white Gaussian noise with SNR=0db. The values for directional textures are shown by solid bars, for the isotropic textures are shown by dashed bars, and the error means are shown by dotted bars. The textures D19, D22, D56, D76 and D102 have higher errors compared with other directional textures due to either multiple principal directions or weak staight lines that are significantly affected by the additive noise.

To evaluate the robustness of the proposed method to illumination, we changed the illuminations of the images by multiplying a 2-D Gaussian function shown in Fig. 12. The principal directions were estimated using the proposed method before and after changing the illumination. Defining the error as the difference between these two estimations, the means and SRMS of errors are presented in Fig. 13. As shown, the illumination does not have significant effect on the orientation estimation of directional textures. In this figure, the mean and standard deviation of the SRMS of errors for the directional textures are 1.97° and 4.77°, respectively. The textures D22, D56, D76 and D102 have larger errors due to either multiple principal directions or weak staight lines affected by illumination.

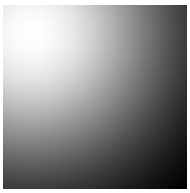

Fig. 12. The 2-D Gaussian function for changing the illumination.

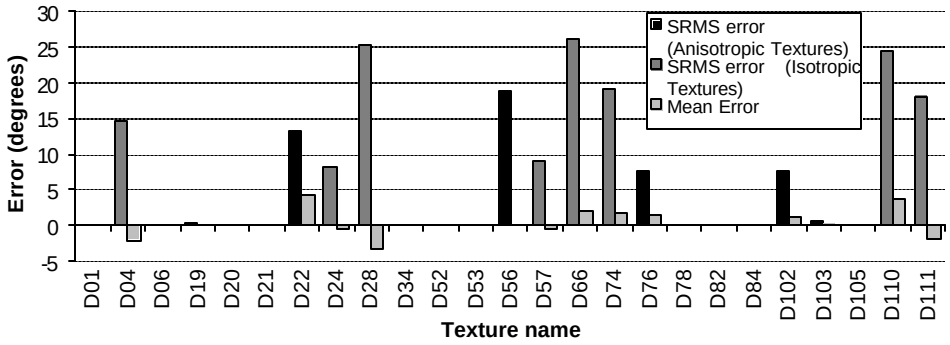

Fig. 13. The SRMS and means of differences between the estimated orientations before and after changing the illumination. The values for directional textures are shown by solid bars, for the isotropic textures are shown by dashed bars and the error means are shown by dotted bars.The textures D22, D56, D76 and D102 have larger errors compared with other directional textures due to either multiple principal directions or weak staight lines affected by illumination.

Data set 2 consists of 24 texture images used in [6]. These texture images are publicly available for experimental evaluation of texture analysis algorithms [32]. We used the 24-bit RGB texture images captured at 100 dpi spatial resolution and illuminant "inca" and converted them to gray-scale images. Each texture is captured at nine rotation angles (0°, 5°, 10°, 15°, 30°, 45°, 60°, 75°, and 90°). Each image is of size 538×716 pixels. Twenty nonoverlapping 128×128 texture samples were extracted from each image by centering a 4×5 sampling grid. We used the angle 0° for training and all the other angles for testing the classifier. Therefore, there are 480 (24×20) training and 3,840 (24×20×8) testing samples. The wavelet transform was calculated using the structure shown in Fig. 14 (30 submatrices, ignoring the HH submatrix of first level of decomposition). Wavelet features were calculated for each submatrix using (3). Table 4 shows the error results using five different wavelet bases and different number of neighbors for *k*-NN

classifier before and after applying the weights. As shown in this table, the maximum correct classification percentage (CCP) is 96.0%. The results using local binary pattern are presented in Table 5. As shown, the maximum classification rate is also 96.0% using 10+26=36 features. Ojala et al. [6] have achieved a classification rate of 97.9% using a joint distribution of features $LBP_{P,R}^{riu2} / VAR_{P,R}$ for (P,R) values of (8,1) and (24,3), and a 3-NN classifier with dissimilarity measurement using a nonparametric statistical test. However, the total number of features is $10B_1+26B_2$ where B_1 and B_2 are the number of bins selected for $VAR_{8,1}$ and $VAR_{24,3}$, respectively. The numbers of bins B_1 and B_2 have not been mentioned for this data set, but obviously $10B_1+26B_2$ is much greater than 30. A classification rate of 97.4% has been reported in [19] using the same data set and 32 features.

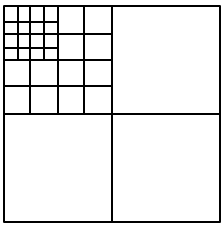

Fig. 14. The wavelet decomposition structure for data set 2.

Table 4. The correct classification percentages for data set 2 using the proposed method with feature e_1, different wavelet bases, and different k values in k-NN classifier.

Wavelet Bases	Features	k					
		1	3	5	1	3	5
		Before Weight			After Weight		
db_2	e_1	92.7	91.1	90.0	94.2	92.4	91.8
db_4	e_1	93.4	91.9	91.0	95.3	93.8	92.9
db_6	e_1	94.0	92.4	91.3	**96.0**	94.0	93.1
db_8	e_1	93.5	92.2	91.5	95.2	93.8	93.0
db_{12}	e_1	93.4	91.9	90.7	94.8	93.5	92.5

Table 5. The correct classification percentages for data set 2 using local binary patterns and different k values in k-NN classifier.

Feature	P,R	k					
		1	3	5	1	3	5
		Before Weight			After Weight		
$LBP_{P,R}^{riu2}$	8,1	74.0	73.8	73.3	73.4	72.3	71.7
	16,2	87.0	85.9	85.6	88.7	87.2	86.3
	24,3	92.3	91.9	91.1	92.5	92.8	92.4
	8,1+16,2	88.9	88.1	87.3	90.3	89.1	88.6
	8,1+24,3	**96.0**	95.7	94.9	95.8	95.8	95.3
	16,2+24,3	94.3	93.8	92.8	95.6	94.8	94.4
	8,1+16,2+24,3	95.5	94.9	94.5	95.8	95.7	95.3

Data set 3 consists of 60 texture images of size 512×512 from the Brodatz album. These texture images are displayed in Fig. 15. The training and testing sets were created in the same way as for data set 1, yielding a total of 240 (60×4) images for training and 3,840 (60×4×16) images for testing (approximately 6% for training and 94% for testing). The experiments were also done as for data set 1. Table 6 shows the CCPs using four different wavelet bases and different number of neighbors for the *k*-NN classifier. The results are reported before and after applying the weights on the features. As shown, the maximum CCP is 96.7%. Data set 3 contains most of the 15 textures used in [18] (except D29 and D69). A classification rate of 84.6% has been reported in [18] while different orientations of the textures have been used in the training phase. However, in our experiments only non-rotated textures have been used for training. Nevertheless, a direct comparison with the method in [18] is not possible due to the difference between the classifiers.

Table 7 and Fig. 16 show the confusion maps and errors for the maximum classification rate of 96.7% in Table 6. To minimize their sizes, only the textures with non-zero error have been shown.

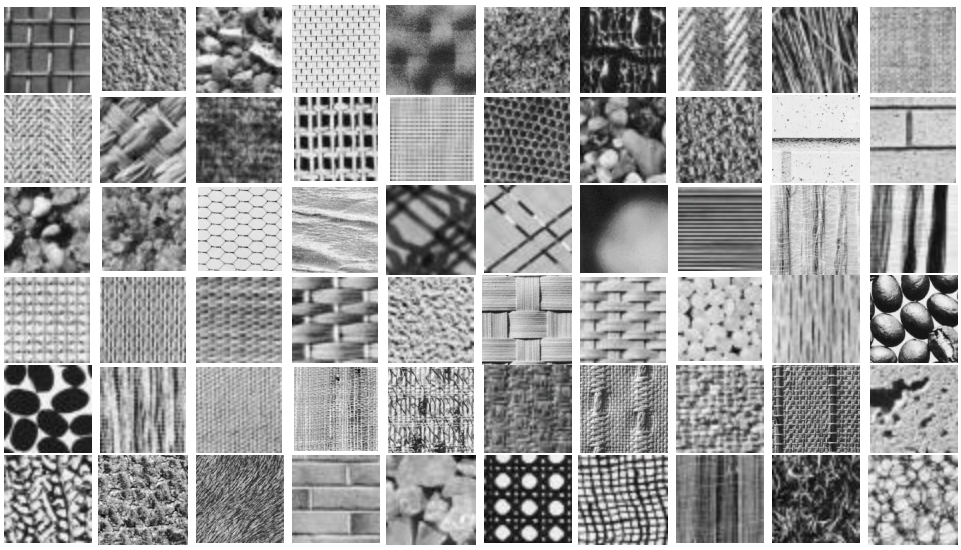

Fig. 15. The 60 textures from the Brodatz album used in data set 3. First row: D01, D04, D05, D06, D08, D09, D10, D11, D15, D16. Second row: D17, D18, D19, D20, D21, D22, D23, D24, D25, D26. Third row: D27, D28, D34, D37, D46, D47, D48, D49, D50, D51. Fourth row: D52, D53, D55, D56, D57, D64, D65, D66, D68, D74. Fifth row: D75, D76, D77, D78, D81, D82, D83, D84, D85, D86. Sixth row: D87, D92, D93, D94, D98, D101, D103, D105, D110, D111.

Table 8 shows the classification rates using wavelet db_4 features for the 20 isotropic textures from data set 3 (D04, D05, D09, D10, D23, D24, D27, D28, D37, D48[2], D57, D66, D74, D75, D86, D87, D92, D98, D110, and D111). Compared with Table 6, the classification rate is lower for the isotropic textures.

[2] For 128×128 images, D48 is non-directional.

Table 6. The correct classification percentages for data set 3 using the proposed method with different wavelet bases, feature sets, and k values in k-NN classifier.

Wavelet Bases	Features	k					
		1	3	5	1	3	5
		Before Weight			After Weight		
db_2	e_1	88.6	81.9	76.9	91.5	84.5	73.5
	e_2	61.2	52.0	52.9	69.2	59.9	59.2
	e_1 & e_2	93.4	88.0	84.6	96.6	92.8	85.3
db_4	e_1	89.3	83.9	77.2	92.2	86.1	74.7
	e_2	64.9	55.5	57.4	68.4	59.4	60.4
	e_1 & e_2	94.4	90.1	85.8	**96.7**	93.2	85.4
db_6	e_1	89.3	83.3	76.7	91.8	85.5	73.5
	e_2	55.4	43.5	44.7	58.9	50.1	52.3
	e_1 & e_2	92.9	86.4	81.8	96.5	91.8	84.7
db_8	e_1	90.5	85.0	78.6	92.5	86.5	75.5
	e_2	45.0	33.5	37.7	52.9	43.3	45.1
	e_1 & e_2	87.4	81.0	77.1	95.9	90.8	84.4
db_{12}	e_1	87.2	80.7	74.9	90.5	85.1	75.1
	e_2	37.8	26.1	28.8	47.0	39.4	41.7
	e_1 & e_2	80.5	70.2	65.5	93.5	90.8	82.8

Table 7. The distribution of errors for the maximum classification rate of 96.7% in Table 6. In this table, only the textures with non-zero error are shown.

	D04	D05	D08	D09	D11	D15	D18	D19	D20	D21	D22	D23	D24	D26	D27	D28	D37	D46	D50	D55	D77	D84	D86	D87	D92	D94	D98	D105	D111
D04	59			5																									
D05		62										1				1													
D15				5		59																							
D18							59					1			3												1		
D19								62								1									1				
D20									62													1	1						
D21										63											1								
D22											63													1					
D23		2										42			12												8		
D24	20												44																
D26														63												1			
D27												5			53												6		
D37																	55									1	8		
D46			1															63											
D50																			61							3			
D55					20															44									
D92		1														1									62				
D94																			2							62			
D98															1												63		
D105																	2		7									55	
D111																							2						62

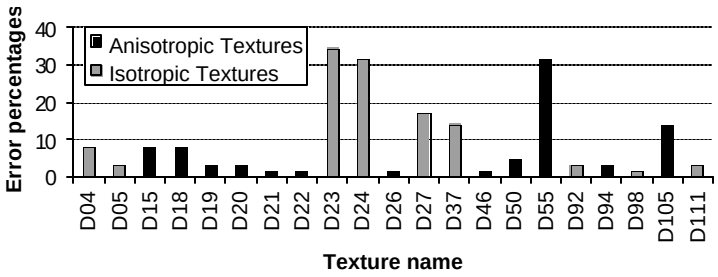

Fig. 16. The errors for the maximum classification rate of 96.7% in Table 6. In this figure only the textures with non-zero error are shown.

Table 8. The correct classification percentages for isotropic textures of data set 3 using the proposed method with db_4 wavelet, different feature sets and k values in k-NN classifier.

Wavelet Basis	Features	k					
		1	3	5	1	3	5
		Before Weight			After Weight		
db_4	e_1	84.0	80.0	74.2	86.4	81.9	75.2
	e_2	54.2	42.9	44.3	56.1	45.4	46.9
	e_1 & e_2	91.0	88.4	84.5	94.3	90.3	84.3

V. CONCLUSION

We have introduced a new technique for rotation invariant texture analysis using Radon and wavelet transforms. In this technique, the principal direction of the texture is estimated using Radon transform and then the image is rotated to place the principal direction at 0°. Next, wavelet transform is employed to extract the features. The method for estimation of the principal direction is shown to be robust to additive white noise and illumination variations. We did a comparison with two of the most recent rotation invariant texture analysis techniques. Experimental results show that the proposed method is comparable to or outperforms these methods while using a smaller number of features.

Although the proposed method for principal direction estimation is suitable for most of the ordinary textures, more complex textures may need more complex techniques. For example, some textures may have straight lines along several directions. This may create ambiguity for the direction estimation. In this situation, more complex methods may be employed to estimate the direction. To make the method invariant to other geometric distortions, the second part of the method, i.e., the feature extraction method can be modified.

REFERENCES

[1] J. Zhang and T. Tan, "Brief review of invariant texture analysis methods," *Pattern Recognition*, vol. 35, pp. 735-747, 2002.

[2] L. S. Davis, "Polarogram: a new tool for image texture analysis," *Pattern Recognition*, vol. 13, no.3, pp. 219-223, 1981.

[3] R.L. Kashyap and A. Khotanzad. "A Model-Based Method for Rotation Invariant Texture Classification," *IEEE Trans. Pattern Anal. Machine Intell.*, vol. 8, pp. 472-481, 1986.

[4] J. Mao, A.K. Jain, "Texture classification and segmentation using multiresolution simultaneous autoregressive models," *Pattern Recognition*, vol. 25, no. 2, pp. 173-188, 1992.

[5] M. Pietikainen, T. Ojala and Z. Xu, "Rotation-invariant texture classification using feature distributions," *Pattern Recognition*, vol. 33, pp. 43-52, 2000.

[6] T. Ojala, M. Pietikainen, and T. Maenpaa, "Multiresolution gray-scale and rotation invariant texture classification with local binary patterns," *IEEE Trans. Pattern Anal. Machine Intell.*, vol. 24, no. 7, pp. 971-987, July 2002.

[7] G. Ravichandran, M.M. Trivedi, "Circular-Mellin features for texture segmentation," *IEEE Trans. Image Processing*, vol. 4, no. 12, pp. 1629–1640, Dec. 1995.

[8] W. Lizhi, G. Healey, "Using Zernike moments for the illumination and geometry invariant classification of multispectral texture," *IEEE Trans. Image Processing*, vol. 7, no. 2, pp. 196–203, 1998.

[9] H. Greenspan, S. Belongie, R. Goodman, and P. Perona, "Rotation invariant texture recognition using a steerable pyramid," in *Proc. Int. Conf. on Pattern Recognition*, Conference B: Computer Vision & Image Processing. , 1994, vol. 2, pp. 162-167.

[10] F.S. Cohen, Z. Fan and M.A. Patel, "Classification of rotated and scaled textured images using Gaussian Markov random field models," *IEEE Trans. Pattern Anal. Machine Intell.*, vol. 13, no. 2 , pp. 192–202, Feb. 1991.

[11] J.-L. Chen and A. Kundu, A. "Rotation and gray scale transform invariant texture identification using wavelet decomposition and hidden Markov model," *IEEE Trans. Pattern Anal. Machine Intell.*, vol. 16, no. 2, pp. 208–214, Feb. 1994.

[12] C.-M. Pun; M.-C. Lee, "Log-polar wavelet energy signatures for rotation and scale invariant texture classification," *IEEE Trans. Pattern Anal. Machine Intell.*, vol. 25, no. 5, pp. 590–603, May 2003.

[13] R. Manthalkar, P.K. Biswas, and B.N. Chatterji, "Rotation and scale invariant texture features using discrete wavelet packet transform," *Pattern Recognition Letters*, vol. 24, pp.2455-2462, 2003.

[14] D. Charalampidis and T. Kasparis, "Wavelet-based rotational invariant roughness features for texture classification and segmentation," *IEEE Trans. Image Processing*, vol. 11, no. 8, pp. 825–837, Aug. 2002.

[15] G.M. Haley and B.S. Manjunath, "Rotation-invariant texture classification using a complete space-frequency model," *IEEE Trans. Image Processing*, vol. 8, no. 2, pp. 255–269, 1999.

[16] W.-R. Wu and S.-C. Wei, "Rotation and gray-scale transform-invariant texture classification using spiral resampling, subband decomposition, and hidden Markov model," *IEEE Trans. Image Processing*, vol. 5, no. 10, pp. 1423–1434, Oct. 1996.

[17] M. N. Do and M. Vetterli, "Rotation invariant characterization and retrieval using steerable wavelet-domain hidden Markov models," *IEEE Trans. Multimedia*, vol. 4, no. 4, pp. 517-526, Dec. 2002.
[18] P. Campisi, A. Neri, G. Panci, and G. Scarano, "Robust rotation-invariant texture classification using a model based approach," *IEEE Trans. Image Processing*, vol. 13, no. 6, pp. 782-791, June 2004.
[19] K. Jafari-Khouzani and H. Soltanian-Zadeh, "Rotation Invariant Multiresolution Texture Analysis Using Radon and Wavelet Transforms," *IEEE Trans. Image Processing*, in Press, 2005.
[20] R. Mester, "Orientation estimation: conventional techniques and a new non-differential approach," in *Proc. 10th European Signal Proc. Conf.*, 2000, vol.2, pp. 921-924.
[21] J. Bigun, G.H. Granlund, and J. Wiklund, "Multidimensional orientation estimation with applications to texture analysis and optical flow," *IEEE Trans. Pattern Anal. Machine Intell.*, vol. 13, no. 8, pp. 775-790, Aug. 1991.
[22] D.V.S. Chandra, "Target orientation estimation using Fourier energy spectrum," *IEEE Trans. Aerosp. Electron. Syst.*, vol. 34, no. 3, pp. 1009-1012, July 1998.
[23] E. Magli, L. Lo Presti, and G. Olmo, "A pattern detection and compression algorithm based on the joint wavelet and Radon transform," in *Proc. IEEE 13th Int. Conf. Digital Signal Processing*, 1997, vol. 2, pp. 559-562.
[24] A.L. Warrick and P.A. Delaney, "Detection of linear features using a localized Radon transform with a wavelet filter," in *Proc. ICASSP*, 1997, vol. 4, pp. 2769-2772.
[25] V.F. Leavers, "Use of the two-dimensional Radon transform to generate a taxonomy of shape for the characterization of abrasive powder particles," *IEEE Trans. Pattern Anal. Machine Intell.*, vol. 22, no. 12, pp. 1411-1423, Dec. 2000.
[26] M.N. Do and M. Vetterli, "The finite ridgelet transform for image representation," *IEEE Trans. Image Processing*, vol. 12, no. 1, pp. 16-28, Jan. 2003.
[27] Jean-Luc Starck, E.J. Candes, and D.L. Donoho, "The curvelet transform for image denoising," *IEEE Trans. Image Processing*, vol. 11, no. 6, pp. 670-684, June 2002.
[28] Bracewell, and Ronald N, *Two-Dimensional Imaging*. Englewood Cliffs, NJ: Prentice Hall, 1995.
[29] E. Gose, R. Johnsonbaugh, and S. Jost, *Pattern Recognition and Image Analysis*, NJ: Prentice Hall, 1996.
[30] A. Averbuch, R.R. Coifman, D.L. Donoho, M. Elad, and M. Israeli, "Accurate and fast discrete polar fourier transform," in *Proc. 37th Asilomar Conf. Signals, Systems & Computers*, 2003, vol. 2, pp. 1933-1937.
[31] P. Brodatz, *Texture: A Photographic Album for Artists and Designers.* New York: Dover, 1966.
[32] http://www.outex.oulu.fi/